Motion Guides for Assisted Manipulation

Kevin M. Lynch
Caizhen Liu
Allan Sørensen
Songho Kim
Michael Peshkin
J. Edward Colgate
Tanya Tickel
David Hannon
Kerry Shiels

Mechanical Engineering Department
Northwestern University
Evanston, IL 60208, USA

Motion Guides for Assisted Manipulation

Kevin M. Lynch, Caizhen Liu, Allan Sorensen, Songho Kim, Michael Peshkin,

Ed Colgate, Tanya Tickel, David Hannon, Kerry Shiels

International Journal of Robotics Research, 21(1), January 2002, p.27-43

Abstract

This paper explores the use of passive guides to assist a human in manipulating heavy loads. A guide acts as a frictionless rail which confines the load to a one-dimensional curve in its configuration space. In this paper we formulate the problem of designing guides to effectively assist the human, and we apply the formulation to two types of materials handling tasks: pushing a heavy cart and single-arm reaching motions. Guides may be implemented by fixed rails or programmable constraint machines. Initial experiments with humans suggest the potential benefits of guided manipulation.

KEY WORDS—human-robot cooperation, programmable constraints, ergonomics, optimal motion guides, constrained motor control

1. Introduction

This paper examines a simple idea: the use of passive guides to assist a human in manipulating heavy loads. A guide acts as a frictionless rail which confines the load to a one-dimensional curve in its configuration space. This is a type of collaborative manipulation: the human and the guide cooperate to move the load from one configuration to another. The guide may be implemented by a fixed rail, but preferably by a programmable constraint machine, such as a cobot (Peshkin et al. 2000).

Unlike approaches to robot-assisted manipulation based on human force amplification, a guide is a passive device; it redirects the momentum of the load without affecting the energy. A drawback is that this limits the set of tasks to which the approach is applicable. Advantages are that guides may be inexpensive to implement, the passivity of guides makes them inherently safe for human collaboration, and stability problems characteristic of force feedback with limited bandwidth are avoided. By designing the guide properly, we allow the operator to use large muscle groups to provide forces in directions that are comfortable while the guide directs the motion to the goal configuration. This approach combines the strengths of the operator (the ability to monitor the progress of the task and to stop the motion in an emergency) with the precise positioning and ergonomic benefits provided by the guide.

While a motion guide certainly reduces the need for tedious fine positioning of the load, our focus in this paper is on reducing operator strain. Our final goal is to design guides to minimize the risk of work-related musculoskeletal disorders (WMSD's) in repetitive manual materials handling. Manual materials handling exposes the worker to known risk factors for WMSD's, such as lifting, bending, twisting, pulling, pushing, and maintenance of static postures. Workplace injuries cost US industry billions of dollars a year, and many of these injuries are from cumulative trauma. In 1990 the average worker's compensation bill for a lost-time back injury was $24,000 (National Council on Compensation Insurance data), and estimates from Ford Motor Co. place the cost of workplace injury at 50 cents per hour worked.

In this paper we formulate the problem of designing frictionless motion guides to help a human manipulate a load more comfortably. The problem is a path planning problem with an objective function quantifying human effort or strain. We apply the formulation to two example tasks: manipulation of a heavy load on a push-cart and repetitive arm reaching motions. The first task is relevant because about 20% of exertion injuries in the USA can be attributed to pushing and

The International Journal of Robotics Research
Vol. 21, No. 1, January 2002, pp. 27-43,

pulling activities (National Institute for Occupational Safety and Health 1981). The second task has been heavily studied in the human motor control literature, allowing us to draw on previously proposed objective functions for reaching motions.

The purpose of this paper is to formulate the constrained manipulation problem and to demonstrate the benefit of guided manipulation using simple objective functions for two different tasks. Future experimental work is needed to further our understanding of objective functions capturing the notion of effort or strain in various materials handling tasks.

Section 2 reviews related work. Section 3 formulates the guide design problem, and Sections 4 and 5 apply the formulation to the two different task domains. Section 6 describes several avenues of further research.

2. Related Work

Our work draws inspiration from previous work in robot-assisted manipulation, ergonomic materials handling, and optimal human motions. We review some of the relevant work below.

2.1. Robot-Assisted Manipulation

This paper studies a novel method of human-robot interaction, where the robot acts as a passive guide. Three other forms of assisted manipulation which have been studied in robotics are teleoperation, human power assist, and human-robot coordinated manipulation. Teleoperation is the most mature of these areas, but we will not review it here. In teleoperation the user does not share a workspace with the robot, and transmitting sensory information to the human is an important issue.

Power assist. Kazerooni (1990, 1996) has pioneered the development of human manipulator "extenders" which amplify human force capabilities. In one example, the human operator physically attaches her arm to a hydraulic device which can sense and amplify the forces applied by the operator. The stability of human-robot systems is studied by Kosuge et al. (1993). Hayashibara et al. (1997) built a 2DoF power assist robot arm to amplify the torques at the human shoulder and elbow in a vertical plane. Force compensation for gravitational and dynamic loads can be adjusted separately. Homma and Arai (1995) and Nagai et al. (1998) have developed robotic orthoses to assist arm motion for disabled people.

Human-robot coordinated manipulation. In human-robot coordinated manipulation, the human is not directly attached to the robot; instead, the human and robot are attached to the load and interact through it (Yamamoto et al. 1996, Al-Jarrah and Zheng 1996, Kim and Zheng 1998). Manipulation forces are distributed between the human and the robot. The robot must have some form of compliance control, and it should be able to interpret the human's intentions in terms of the forces sensed at the robot's end-effector. Recently Arai et al. (2000) and Takubo et al. (2000) have used a robot simulating a nonholonomic constraint to act like a virtual wheelbarrow for intuitive human-robot collaboration.

In both of the approaches above, as with our approach, the human and the robot share a workspace, and the human provides the sensing and intelligence to monitor the task. In power-assist and human-robot coordinated manipulation, however, difficult sensing and control issues arise to maintain the safety and stability of the system with a reasonable control bandwidth. Because our approach to assisted manipulation uses passive guides or programmable constraint machines, these issues are avoided.

Cobots (Peshkin et al. 2000) are programmable constraint machines which provide smooth, rigid constraints through steerable rolling contacts, and they are a good candidate to implement the guides designed in this paper. While conventional robots may in principle be used to set up motion guides, doing so requires that the motors be strong enough to resist operator and payload inertial forces that would penetrate the guides. Such powerful motors may pose safety problems. Also, in practice, the performance of such virtual surfaces (e.g., their smoothness) has proven to be poor.

2.2. Ergonomic Materials Handling

The study of WMSD's, and specifically low back disorders, can be broadly classified into two categories: psychophysical and biomechanical/physiological. In psychophysical studies, subjects are typically asked to perform materials handling tasks with frequencies and weights that they can sustain for an eight hour day without overexertion. Biomechanical studies of the spine relate task forces to compression and shear loads on the spine.

A review of the psychophysical methodology is given by Ayoub and Dempsey (1999). This approach has resulted in a large database of guidelines for designing lifting, lowering, pushing, pulling, and carrying tasks for men and women (Snook and Ciriello 1991, see also the National Institute for Occupational Safety and Health guidelines 1981). Safe lifting tasks have been studied by Legg and Myles (1981) and Mital (1983). Maximum and sustained comfortable forces in pushing and pulling a cart have been studied by Ciriello et al. (1999) and Al-Eisawi et al. (1999). Examples of the biomechanical approach to ergonomics include studies on compressive, shear, and torsional loads on the spine (Brinkman 1986, Shirazi-Adl et al. 1986, Adams and Hutton 1983). Marras et al. (1999) showed that spine loading during lifting of a box depends on the location of the grasp on the box. Granata and Marras (1999) demonstrated that shear and torsional loads on the spine (for instance from twisting), not just compressive loads, are important factors in low back disorders.

2.3. Optimal Human Motions

Normal human limb motions have a grace and efficiency that have inspired researchers to hypothesize that these motions minimize some measure of effort. For human arm (shoulder and elbow) point-to-point motions, two popular models are minimum Cartesian jerk at the hand (Flash and Hogan 1985) and minimum rate of change of torque at the shoulder and elbow joints (Uno et al. 1989), both of which predict unconstrained arm trajectories similar to those measured by Morasso (1981) and Abend et al. (1982). Todorov and Jordan (1998) present evidence that natural arm movements along curved paths tend to minimize jerk. Alexander (1997) calculated arm trajectories to minimize metabolic cost of the motion, based on a model of muscle metabolic rates (Ma and Zahalak 1991), and showed that the resulting trajectories closely match experimental trajectories found by Hollerbach and Atkeson (1987). Harris and Wolpert (1998) propose that minimization of the variance of the arm's position in the presence of biological noise is a key factor in motor control.

The smooth trajectories predicted by these objective functions may also be due to mechanical filtering properties intrinsic to muscle tissue. This possibility is studied by Hogan (1985) and Krylow and Rymer (1997). Gomi and Kawato (1995, 1996, 1997) have studied the stiffness of the human arm during point-to-point motion with and without guiding constraints.

For large-scale manipulation of large loads, locomotion is involved. Kram (1998) presents evidence that for a given speed of motion, animals tend to choose the gait (e.g., walking/trotting/galloping) that minimizes the metabolic cost.

These works provide insight into natural unconstrained human motion. Efficiency criteria for constrained motion may be different than those for unconstrained motion.

3. Problem Formulation

In this section we provide a general formulation of the optimal guide design problem for assisted manipulation, and we apply the formulation to two specific examples in Sections 4 and 5.

The load being manipulated is a rigid three-dimensional body. A frictionless guide constrains the load to move along a one-dimensional curve in its configuration space. The guide may be implemented by a fixed guide rail or a cobot.

We define an inertial frame $\mathcal{F}^w$ and a body frame $\mathcal{F}^b$ fixed to the center of mass of the load. The configuration of $\mathcal{F}^b$ relative to $\mathcal{F}^w$ at time t is written

$$g(t) = \begin{bmatrix} R(t) & \mathbf{p}(t) \\ \mathbf{0}_{1\times 3} & 1 \end{bmatrix} \in SE(3),$$

where $R(t) \in SO(3)$ is the 3×3 rotation matrix giving the orientation of $\mathcal{F}^w$ in $\mathcal{F}^b$ and $\mathbf{p}(t) \in \Re^3$ is the vector from the origin of $\mathcal{F}^w$ to the origin of $\mathcal{F}^b$, measured in $\mathcal{F}^w$.

We may represent the velocity of $\mathcal{F}^b$ relative to $\mathcal{F}^w$ by the pair $(\dot{R}, \dot{\mathbf{p}})$, or, using the 3×1 angular velocity vector ω of $\mathcal{F}^b$ in $\mathcal{F}^w$, as an element of $se(3)$:

$$\begin{bmatrix} \hat{\omega} & \dot{\mathbf{p}} \\ 0 & 0 \end{bmatrix} \in se(3), \quad \text{where } \hat{\omega} = \begin{bmatrix} 0 & -\omega_3 & \omega_2 \\ \omega_3 & 0 & -\omega_1 \\ -\omega_2 & \omega_1 & 0 \end{bmatrix},$$

where $\dot{R} = \omega \times R = \hat{\omega}R$. For compactness, we write the velocity as the 6×1 vector $\mathbf{v} = (\dot{\mathbf{p}}^T, \omega^T)^T$.

The mass of the rigid body is m. The (constant) positive semi-definite inertia matrix is I^b in $\mathcal{F}^b$ and $I = RI^bR^T$ when measured in a frame aligned with $\mathcal{F}^w$ at the load center of mass. The Newton–Euler equations for the rigid body can be written

$$\mathbf{f} = m\ddot{\mathbf{p}} \tag{1}$$

$$\tau = I\dot{\omega} + \omega \times I\omega, \tag{2}$$

where $\mathbf{f}$ is the force applied at the center of mass in $\mathcal{F}^w$ and the torque τ is measured about the center of mass of the load in a frame aligned with $\mathcal{F}^w$. The forces and torques may be written as a 6×1 wrench vector $\mathbf{w} = (\mathbf{f}^T, \tau^T)^T$.

The total wrench $\mathbf{w}$ applied to the load is the sum $\mathbf{w} = \mathbf{w}_n + \mathbf{w}_t$, where $\mathbf{w}_n$ and $\mathbf{w}_t$ are orthogonal ($\mathbf{w}_n^T\mathbf{w}_t = 0$) and $\mathbf{w}_n$ belongs to the five-dimensional subspace of workless wrenches $\{\mathbf{w} | \mathbf{w}^T\mathbf{v} = 0\}$. The wrench along the path is written $\mathbf{w}_t = A(\mathbf{v})\mathbf{w}$, where $A(\mathbf{v}) = \mathbf{v}\mathbf{v}^T/||\mathbf{v}||^2$. We will refer to $\mathbf{w}_n$ as the wrench "normal" to the path and $\mathbf{w}_t$ as the wrench "tangential" to the path.

We may also write $\mathbf{w} = \mathbf{w}_g + \mathbf{w}_h + m\mathbf{g}$, where $\mathbf{w}_g$ is the wrench due to the motion guide, $\mathbf{w}_h$ is the wrench due to the human, and $m\mathbf{g}$ is the gravitational wrench (with zero torque components). Because the frictionless guide is a workless constraint, the guide wrench $\mathbf{w}_g$ is always normal to the path ($\mathbf{w}_g^T\mathbf{v} = 0$). The human wrench $\mathbf{w}_h$ may be written as the sum of normal and tangential components $\mathbf{w}_h = \mathbf{w}_{h,n} + \mathbf{w}_{h,t}$, where $\mathbf{w}_{h,t} = A(\mathbf{v})\mathbf{w}_h$.

The configuration of the human during the manipulation is written $h(t)$. In general, $h = (h_j, h_c) \in \mathcal{M} \times SE(3)$, where $h_j \in \mathcal{M}$ represents the joint configuration of the body (the "shape" of the body) and $h_c \in SE(3)$ gives the configuration of a frame fixed in the human body relative to $\mathcal{F}^w$. During manipulation, $g(t)$ and $h(t)$ must satisfy a set of constraints of the form $f(g(t), h(t)) = 0$, ensuring that the human stays in contact with the load. The human configuration $h(t)$ must also satisfy a number of other complex constraints based on biomechanics and simple physical laws; e.g., the human cannot simply float above the floor during a locomotion task. It is impractical, however, to consider the entire configuration of the human body during manipulation. In this paper, we focus on systems with simple relationships between $g(t)$ and $h(t)$. For example, in the guided arm motions of Section 5, the arm configuration is derived from the load configuration

$g(t)$ by the one-to-one mapping of the arm inverse kinematics, assuming the torso is fixed.

The problem can now be formulated: Given an initial state $(g_0, \mathbf{v}_0)$ and goal state $(g_1, \mathbf{v}_1)$ for the load and a desired cycle time t_f, find $g(t), h(t)$, and $\mathbf{w}_h(t)$ satisfying $g(0) = g_0$, $\mathbf{v}(0) = \mathbf{v}_0$, $g(t_f) = g_1$, $\mathbf{v}(t_f) = \mathbf{v}_1$, the equations of motion (eqs. (1) and (2)), and any constraints on $h(t)$, while minimizing an objective function

$$c = \int_0^{t_f} J(g(t), h(t), \mathbf{w}_h(t))dt, \tag{3}$$

where the dependence on $g(t)$, $h(t)$, and $\mathbf{w}_h(t)$ may include time derivatives of these functions. Then the path associated with $g(t)$ defines the optimal motion guide and speed along the path, and $h(t)$ and $\mathbf{w}_h(t)$ define the optimal human interaction with the guide.[1]

The objective function c encodes our notion of natural or comfortable manipulation. It only penalizes the wrenches $\mathbf{w}_h(t)$ provided by the human; wrenches provided by the motion guide and gravity are free. This is because our goal is to make the manipulation as comfortable as possible for the human. The objective function can also penalize certain regions of the load or body state space, perhaps to avoid obstacles or high speeds where the human has difficulty keeping up with the motion.

It is important to keep in mind that an "optimal" guide is tied up with the chosen objective function. A great deal of previous work in human motor control has shown that many human motions are stereotypical, suggesting an organizing principle (which can be expressed as a cost function) common across most normal subjects (Section 2.3). If experimental records of human interaction with a guide closely match those predicted in the minimization of eq. (3), then this is evidence that the objective function is a good description of the organizing principle. Throughout this paper we assume that an appropriate objective function has been chosen, so that subjects' natural interaction is optimal by this measure. We call this the *optimal collaboration assumption*. Note that although the total wrench $\mathbf{w}(t)$ and the tangential wrench $\mathbf{w}_t(t)$ are uniquely specified by $g(t)$, and therefore so is the tangential wrench applied by the human

$$\mathbf{w}_{h,t}(t) = \mathbf{w}_t(t) - A(\mathbf{v})m\mathbf{g},$$

the normal portion of the human wrench $\mathbf{w}_{h,n}(t)$ does not affect the motion (since the load is constrained by the guide) and therefore can be chosen arbitrarily in minimizing eq. (3).

This paper does not study in detail the ideal objective functions to describe human interaction with constraints in different tasks, but rather considers simple but plausible objective functions to demonstrate the formulation.

1. The formulation of the problem could also include muscle activation levels, which are not completely determined by $g(t)$, $h(t)$, and $\mathbf{w}_h(t)$.

4. Example: Planar Manipulation with a Cobot Cart

We now apply the problem formulation of Section 3 to collaborative manipulation in a horizontal plane. For concreteness, we assume the load is rigidly attached to a tricycle cobot cart (Figure 1). The human pushes on a handle fixed to the cobot, and the cobot cart controls the steering angles of the wheels to allow motion only along a pre-defined curve. The cobot cart provides a good testbed for the approach, because (1) carts are a common means of manual materials handling, (2) low back strain due to pushing and pulling a cart has been investigated (e.g., Ciriello et al. 1999), and (3) we have a cobot cart prototype in our lab (Wannasuphoprasit et al. 1997). A modified version of this prototype is being tested in a task involving unloading a car door from an assembled car at General Motors.

We nondimensionalize by choosing the unit mass to be the mass of the cobot/load system and the unit distance to be the radius of gyration of inertia, so that $m = I_z = 1$. A body frame $\mathcal{F}^b$ is fixed to the center of mass of the cobot/load system. In the notation of Section 3, the configuration of $\mathcal{F}^b$ in $\mathcal{F}^w$ is written

$$\begin{bmatrix} R & \mathbf{p} \\ \mathbf{0}_{1\times 3} & 1 \end{bmatrix} = \begin{bmatrix} \cos\theta & -\sin\theta & 0 & x \\ \sin\theta & \cos\theta & 0 & y \\ 0 & 0 & 1 & 0 \\ 0 & 0 & 0 & 1 \end{bmatrix}.$$

To express the configuration as an element of $SE(2)$, we simply eliminate the third row and column of the matrix. We more compactly represent the configuration of $\mathcal{F}^b$ as $\mathbf{r} = (x, y, \theta)^T$. The velocity is written $\mathbf{v} = (\dot{x}, \dot{y}, \dot{\theta})^T = \dot{\mathbf{r}}$ and the total wrench is $\mathbf{w} = (f_x, f_y, \tau_z)^T$.

We define a human frame $\mathcal{F}^h$ fixed to the handle of the cobot. The position and orientation of $\mathcal{F}^b$ in $\mathcal{F}^h$ is given by $\mathbf{r}^{hb} = (x^{hb}, y^{hb}, \psi)^T$. To transform the wrench $\mathbf{w}_h$ into a wrench $\mathbf{w}_h^h$ expressed in $\mathcal{F}^h$, we have

$$\begin{aligned} \mathbf{w}_h^h &= T^{hb}T^{bw}\mathbf{w}_h = T^{hw}\mathbf{w}_h \\ &= \begin{bmatrix} \cos\psi & -\sin\psi & 0 \\ \sin\psi & \cos\psi & 0 \\ x^{hb}\sin\psi - y^{hb}\cos\psi & x^{hb}\cos\psi - y^{hb}\sin\psi & 1 \end{bmatrix} \\ &\quad \begin{bmatrix} \cos\theta & \sin\theta & 0 \\ -\sin\theta & \cos\theta & 0 \\ 0 & 0 & 1 \end{bmatrix} \mathbf{w}_h, \end{aligned}$$

where T^{bw} transforms the wrench $\mathbf{w}_h$ into the body frame and T^{hb} transforms from the body to the human frame. The normal and tangential components are written $\mathbf{w}_{h,n}^h = T^{hw}\mathbf{w}_{h,n}$ and $\mathbf{w}_{h,t}^h = T^{hw}\mathbf{w}_{h,t}$, respectively.

To begin our study, we focus on motions beginning and ending at rest, and we choose the objective function to be the

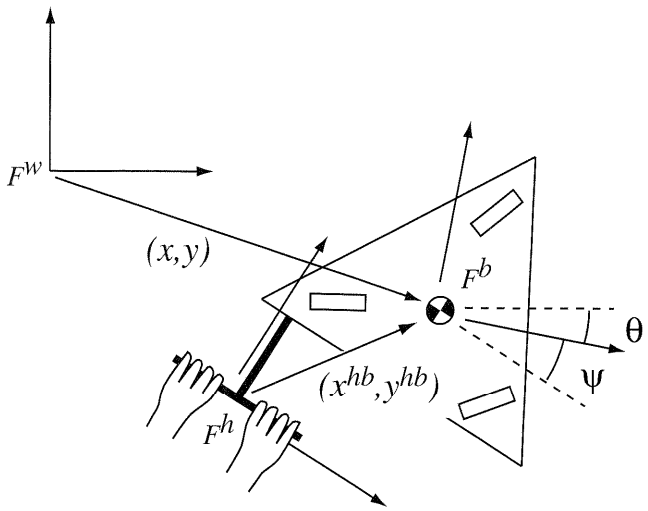

Fig. 1. Model of a tricycle cobot.

integral of a quadratic function of the human wrench $\mathbf{w}_h^h(t)$:

$$c = \int_0^{t_f} \mathbf{w}_h^h(t)^T W \mathbf{w}_h^h(t) dt. \tag{4}$$

This objective function was chosen in part for its simplicity, and in part because there is some evidence that metabolic (input) power is proportional to the square of muscle force output (Nelson 1983, Hogan 1984). In our objective function, the positive semi-definite weight matrix $W = \text{diag}(w_1, w_2, w_3)$ weights the relative cost of the different components of the wrench $\mathbf{w}_h^h$. For instance, awkward twisting and sideways dragging forces could be weighted more heavily than pushing and pulling forces. In this simple objective function we are ignoring factors such as speed of motion and the trajectory of the human body during locomotion. We focus simply on the forces applied by the human.

One notable property of this objective function is that the shape of the optimal guide is independent of the time of motion—the same guide is optimal regardless of how quickly the human performs the motion.

The optimal collaboration assumption for the objective function (eq. (4)) implies that the human chooses a wrench $\mathbf{w}_h^h(t)$ to minimize $\mathbf{w}_h^h(t)^T W \mathbf{w}_h^h(t)$ at all t. Remembering that

$$\mathbf{w}_h^h(t) = \mathbf{w}_{h,t}^h(t) + \mathbf{w}_{h,n}^h(t)$$

and the tangential wrench $\mathbf{w}_{h,t}^h(t)$ is specified by the trajectory $\mathbf{r}(t)$

$$\mathbf{w}_{h,t}^h(t) = T^{hw}(\mathbf{w}_t(t) - A(\mathbf{v})m\mathbf{g}),$$

then the human is free to choose the normal wrench $\mathbf{w}_{h,n}^h(t)$ to minimize $\mathbf{w}_h^h(t)^T W \mathbf{w}_h^h(t)$ for a particular $\mathbf{r}(t)$. We can write the normal wrench

$$\mathbf{w}_{h,n}^h(t) = T^{hw} N(t) \mathbf{a}(t),$$

where the 3×2 matrix $N(t) = (\mathbf{n}_1(t) \mid \mathbf{n}_2(t))$ consists of column vectors $\mathbf{n}_i$ defining a basis for wrenches normal to the path (the set $\{\mathbf{w} | \mathbf{w}^T \mathbf{v}(t) = 0\}$), and the 2-dimensional vector function $\mathbf{a}(t) = (a_1(t), a_2(t))^T$ chooses the normal wrench in $(\mathbf{n}_1, \mathbf{n}_2)$ coordinates. Then $\mathbf{a}(t)$ satisfies the necessary condition for optimal collaboration if

$$\frac{\partial (\mathbf{w}_h^h(t)^T W \mathbf{w}_h^h(t))}{\partial \mathbf{a}(t)} = \mathbf{0} \tag{5}$$

is satisfied for all t.

For a given trajectory $\mathbf{r}(t)$, we can solve eq. (5) for the optimal normal wrench $\mathbf{w}_{h,n}^h(t)$ at each time t. Given a tangential wrench $\mathbf{w}_{h,t}(t) = (f_{hx,t}, f_{hy,t}, \tau_{hz,t})^T$, a basis for the space of normal wrenches is given by $\mathbf{n}_1 = (-f_{hy,t}, f_{hx,t}, 0)^T$ and $\mathbf{n}_2 = (-f_{hx,t}\tau_{hz,t}, -f_{hy,t}\tau_{hz,t}, f_{hx,t}^2 + f_{hy,t}^2)^T$. With this choice of a basis, we can solve eq. (5) for $\mathbf{a}$:

$$a_1 = \frac{(w_1 - w_2) w_3 f_{hx,t} f_{hy,t} (f_{hx,t}^2 + f_{hy,t}^2 + \tau_{hz,t}^2)}{(f_{hx,t}^2 + f_{hy,t}^2)(w_2 w_3 f_{hx,t}^2 + w_1 w_3 f_{hy,t}^2 + w_1 w_2 \tau_{hz,t}^2)}$$

$$a_2 = \frac{(w_2(w_1 - w_3) f_{hx,t}^2 + w_1(w_2 - w_3) f_{hy,t}^2)\tau_{hz,t}}{(f_{hx,t}^2 + f_{hy,t}^2)(w_2 w_3 f_{hx,t}^2 + w_1 w_3 f_{hy,t}^2 + w_1 w_2 \tau_{hz,t}^2)}.$$

Thus, for any load trajectory $\mathbf{r}(t)$, the optimal human force profile $\mathbf{w}_h^h(t)$ follows directly. The problem is to find the optimal load trajectory $\mathbf{r}(t)$. The optimal guide is the associated path.

4.1. Translational Motion

We begin by studying the case of a 2DoF cobot/load with no rotation, $\mathbf{r} = (x, y)^T$. $\mathcal{F}^b$ and $\mathcal{F}^h$ are identical and aligned with $\mathcal{F}^w$. We are interested in the optimal guides from $(0, 0)^T$ to $(x_f, y_f)^T$. The force applied by the human operator is $\mathbf{w}_h^h = \mathbf{w}_h = (f_{hx}, f_{hy})^T$ and the objective function is

$$c = \int_0^{t_f} (w_1 f_{hx}^2(t) + w_2 f_{hy}^2(t)) dt. \tag{6}$$

In the following results, we assume $w_1/w_2 \geq 1$. Intuitively, force in the y direction corresponds to pushing and pulling in the human frame, and force in the x direction corresponds to sideways dragging.

For a tangential wrench $\mathbf{w}_{h,t} = (f_{hx,t}, f_{hy,t})^T$, a basis for the space of normal wrenches is $\mathbf{n}_1 = (f_{hy,t}, -f_{hx,t})^T$. Solving eq. (5), we get

$$a_1 = \frac{(w_1 - w_2) f_{hx,t} f_{hy,t}}{w_2 f_{hx,t}^2 + w_1 f_{hy,t}^2},$$

and an optimal normal wrench $\mathbf{w}_{h,n} = a_1 \mathbf{n}_1$.

We can also interpret the objective function geometrically by recognizing that it defines iso-cost force ellipses in the human frame, as shown in Figure 2. Suppose the human wishes to apply a particular tangential force, as shown in the figure. Since normal forces are canceled by the guide, the human is free to choose any normal force to minimize the cost. In the 2DoF case, this gives a line of human forces in the (f_{hx}, f_{hy}) space which yield the same tangential force. The optimal human force is where this line of equivalent forces is tangent to an iso-cost ellipse. Generalizing the objective function to an n-dimensional wrench space, we have $(n-1)$-dimensional iso-cost wrench ellipsoids and an $(n-1)$-dimensional hyperplane of equivalent wrenches.

4.1.1. Analytical Results

Consider a system described by the nonlinear differential equations

$$\dot{\mathbf{x}} = \mathbf{f}(\mathbf{x}(t), \mathbf{u}(t), t),$$

where $\mathbf{x}$ is the state variable vector and $\mathbf{u}$ is the control vector, and the objective function

$$c = \int_{t_0}^{t_f} J(\mathbf{x}(t), \mathbf{u}(t), t)dt.$$

We define the Hamiltonian

$$H = J(\mathbf{x}(t), \mathbf{u}(t), t) + \lambda(t)^T \mathbf{f}(\mathbf{x}(t), \mathbf{u}(t), t),$$

where $\lambda(t)$ is the Lagrange multiplier vector. Using the calculus of variations (Kirk 1970, Bryson and Ho 1969), we get the necessary condition for optimality

$$\frac{\partial H}{\partial \mathbf{u}} = 0. \tag{7}$$

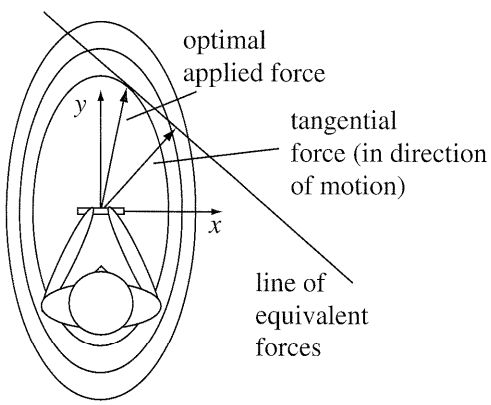

Fig. 2. Iso-cost force ellipses for $w_1/w_2 = 4$.

The Lagrange multiplier vector satisfies the following differential equation:

$$\dot{\lambda} = -\frac{\partial H}{\partial \mathbf{x}}. \tag{8}$$

For the 2DoF cobot, we define the state variables $\mathbf{x} = (x, y, \theta, v)^T$, where $(x, y)^T$ is the configuration of the cobot, v is the speed of the cobot, and θ is the angle of the tangent to the path relative to the x-axis. The control variables are $\mathbf{u} = (\omega, f_t)^T$, where $\dot{\theta} = \omega$ and f_t is the force applied tangential to the path. This yields the state equations $\dot{x} = v\cos\theta$, $\dot{y} = v\sin\theta$, $\dot{\theta} = \omega$, $\dot{v} = f_t$.

Infinite Weight Ratio $w_1/w_2 = \infty$. The weight ratio $w_1/w_2 = \infty$ implies that the cost of pushing and pulling is negligible compared to sideways dragging. The force applied by the human is therefore $(0, f_{hy})^T$, where $f_{hy} = f_t/\sin\theta$, and the objective function is $c = \int_0^{t_f} f_{hy}^2 dt$. The Hamiltonian is

$$H = (f_t/\sin\theta)^2 + \lambda_1\dot{x} + \lambda_2\dot{y} + \lambda_3\dot{\theta} + \lambda_4\dot{v}.$$

We cannot solve eq. (7) analytically for the trajectory $\mathbf{x}(t)$. We can, however, gain insight into the motion at time $t = 0$ and $t = t_f$. For our particular system we have $\partial H/\partial\omega = \lambda_3$, which is zero by condition (7), and therefore $\dot{\lambda}_3 = 0$. Plugging into eq. (8) we have

$$\dot{\lambda}_3 = -\frac{\partial H}{\partial\theta} = \left(\frac{2f_t^2\cos\theta}{\sin^3\theta} + \lambda_1 v\sin\theta - \lambda_2 v\cos\theta\right) = 0.$$

Substituting $v = 0$ at the beginning and end of the motion, we get

$$\frac{f_t^2\cos\theta}{\sin^3\theta} = 0.$$

For the cobot to move, we need $f_t \neq 0$. Therefore, $\cos\theta = 0$ at the beginning and end of the motion. The initial and final motion of the cobot is parallel to the y-axis (see Figure 3).

Goal Configurations $(0, L)^T$. If the goal configuration is of the form $(0, L)^T$ and $w_1/w_2 \geq 1$, clearly the optimal path is the straight line connecting $(0, 0)^T$ and $(0, L)^T$. In this case, a guide provides no ergonomic benefit; we are simply interested in the optimal forces applied by the human. It is easy to show that the optimal force profile $(0, f_{hy}(t))^T$ is a ramp, as shown in Figure 4. The objective function is

$$c = \int_0^{t_f} f_t^2(t)dt = \int_0^{t_f} \dot{v}^2(t)dt,$$

and the speed satisfies

$$L = \int_0^{t_f} v(t)dt,$$

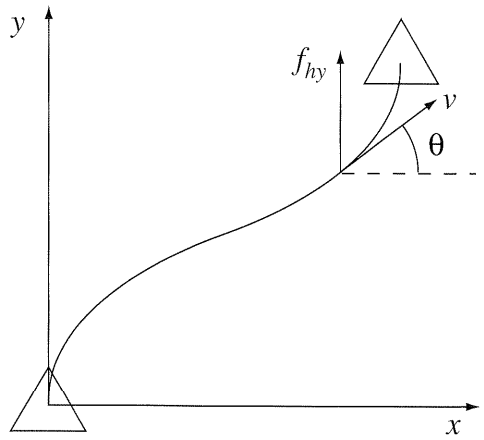

Fig. 3. With an infinite weight ratio w_1/w_2, the tangents to the optimal guide at the initial and goal configurations are parallel to the y-axis.

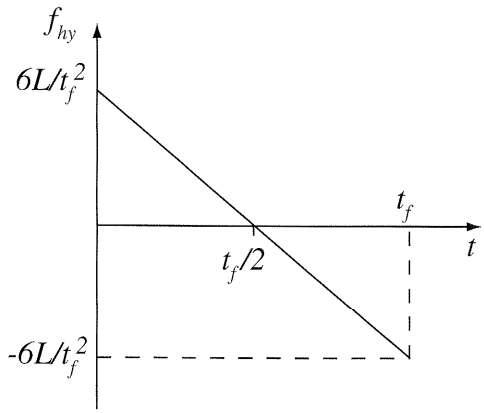

Fig. 4. The optimal human force profile $f_{hy}(t)$ for manipulating a unit mass from $(0, 0)^T$ to $(0, L)^T$ in time t_f.

where L is the distance traveled. The Hamiltonian is

$$H = \dot{v}^2 + \lambda_1 \dot{y} + \lambda_2 \dot{v}.$$

Solving eqs. (7) and (8) and plugging in the boundary conditions $v(0) = v(t_f) = y(0) = 0$, $y(t_f) = L$, we get

$$f_{hy}(t) = \frac{6L}{t_f^2}\left(1 - \frac{2t}{t_f}\right).$$

Equal Force Weights: $w_1/w_2 = 1$. For a weight ratio $w_1/w_2 = 1$, the optimal path to any point is a straight line. The optimal human force profile for interacting with the guide has the same ramp shape as in Figure 4, where the forces applied by the human are tangential to the path.

4.1.2. Numerical Results

To calculate a complete solution for the guide shape, we resort to a numerical approach. The partial analytical results can be used to verify the numerical results.

We represent the cobot trajectory as a polynomial function of time:

$$x(t) = \sum_{i=0}^{n} a_i t^i, \quad y(t) = \sum_{i=0}^{n} b_i t^i, \quad 0 \le t \le t_f.$$

The objective function (eq. (6)) is calculated from a trajectory $(x(t), y(t))^T$ by numerical integration over the trajectory using the optimal collaboration assumption. To solve for the design variables $a_i, b_i, i = 0 \ldots n$ that satisfy the equality constraints $(x(0), y(0))^T = \mathbf{0}$, $(x(t_f), y(t_f))^T = (x_f, y_f)^T$, $(\dot{x}(0), \dot{y}(0))^T = \mathbf{0}$, $(\dot{x}(t_f), \dot{y}(t_f))^T = \mathbf{0}$ and minimize the objective function (eq. (6)), we use CFSQP (Lawrence et al. 1994), a sequential quadratic programming (SQP) solver (Gill et al. 1981). CFSQP allows us to specify arbitrary smooth equality and inequality constraints on the design variables, which we can use to encode constraints other than the boundary conditions.

Given a design variable vector X, SQP requires functions to calculate the constraint values and the objective function, as well as their gradients with respect to X. Although our objective function is calculated numerically, we use the analytical gradient of this approximate objective function. The analytical gradients of the constraints are readily available. The use of analytical gradients, as opposed to finite differences, improves the convergence of the solver.

We present the results of using $n = 8$ in the polynomial trajectories. Since SQP is a local method based on a Newton-Raphson step, an initial guess X_0 is required. To obtain an initial guess, we use the boundary conditions to solve for the low-order coefficients of the polynomial trajectory, setting the higher-order coefficients to zero. For concreteness, in each of the following examples we set $t_f = 1$. The choice of t_f does not affect the shape of the optimal guide. We consider goal configurations on the unit circle; the optimal guide to other points is obtained by scaling.

Effect of the Weight Ratio. Figure 5 shows the optimal guides to the point $(\cos 20°, \sin 20°)^T$ for different weight ratios w_1/w_2. Figures 6 and 7 show the associated optimal human force profiles. They have the features predicted by the analytical results: a large weight ratio means initial and final motion is along the y-axis, and $w_1/w_2 = 1$ implies a straight line guide and a ramp force profile.

The objective function allows us to quantify the benefit of using a guide to assist a motion. We define the benefit to

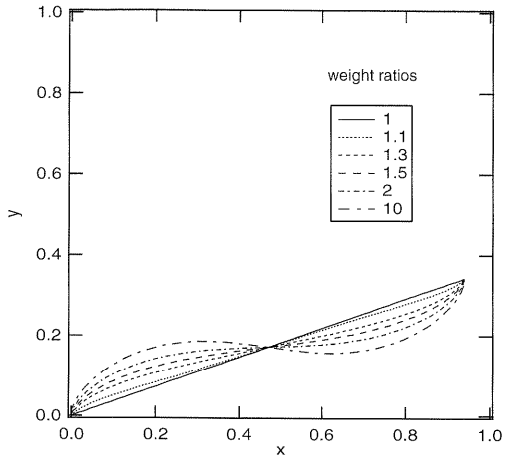

Fig. 5. Optimal guides for different weight ratios w_1/w_2.

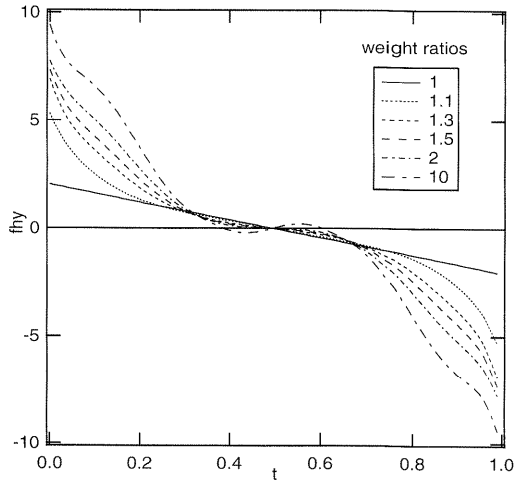

Fig. 7. The f_{hy} component of the optimal human force profiles associated with the guides in Figure 5.

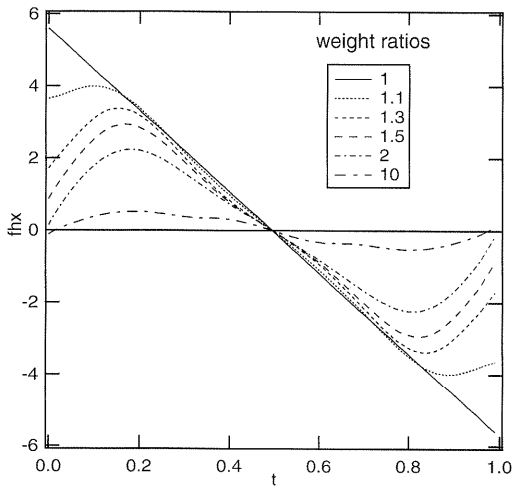

Fig. 6. The f_{hx} component of the optimal human force profiles associated with the guides in Figure 5.

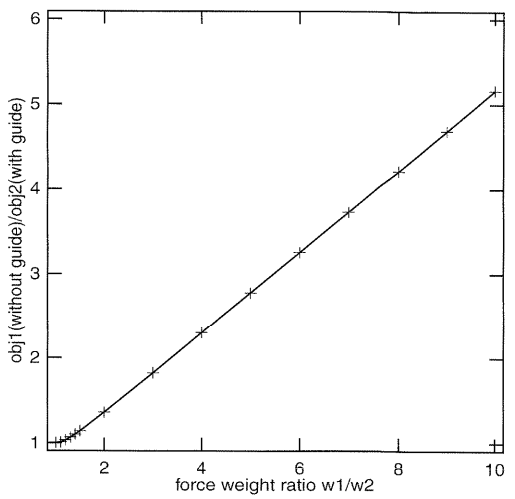

Fig. 8. The benefit of using a guide, as a function of w_1/w_2, to push the load to $(\cos 20°, \sin 20°)$.

be the ratio of the cost of the optimal unguided motion to the cost of the optimal guided motion. The optimal unguided motion simply has the human pushing the load straight to the goal with an optimal (ramp) force profile. Figure 8 shows the benefit as a function of the weight ratio w_1/w_2 for motion to the point $(\cos 20°, \sin 20°)$. As expected, the benefit of the guide increases as the weight ratio increases.

Infinite Weight Ratio. As the weight ratio becomes large, the numerical method shows that the shape of the optimal guides stop changing. This is a useful feature, as the shape of the optimal guide is robust to variations in the weight ratio for large values of the weight ratio. We choose a weight ratio $w_1/w_2 = 1000$ to approximate the case of an infinite weight ratio. Figure 9 shows the optimal guides to points on a unit circle. There are two distinct types of minimizing guides evident in Figure 9, corresponding to different local minima in the design variable space. The figure shows only the globally optimal guides.

4.2. 3DoF Motion

We can apply the same formulation to the case where the cobot/load is allowed to rotate in the plane. For a weight matrix $W = \text{diag}(100, 1, 5)$ and a handle location in the body frame such that $\mathbf{r}^{hb} = (0, 2, 0)^T$, Figure 10 shows the optimal guide from $(0, 0, 0)^T$ to $(0, 5, 0)^T$ (remembering that a unit

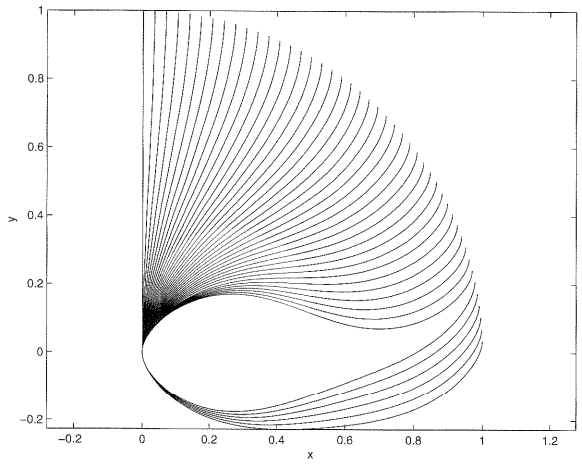

Fig. 9. The optimal guides to points on a unit circle for an infinite weight ratio.

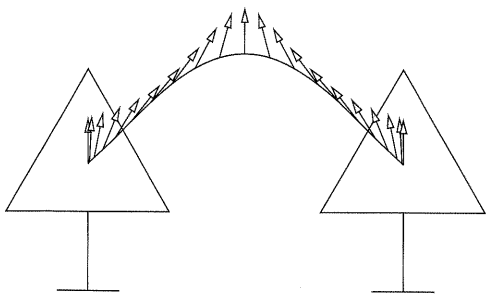

Fig. 10. An optimal guide for planar manipulation with rotation. The guide is specified by the path of the center of mass of the cobot/load and the orientation along the path.

of distance is equal to the radius of gyration of inertia of the cobot/load). The cost to perform this manipulation in 1 s is 426 (units suppressed). Without the ability to rotate (the 2DoF case), the optimal guide yields a cost of 618.

The location of the handle in the body frame may greatly affect the shape and cost of the optimal guide. The elements of $\mathbf{r}^{hb}$ can be treated as design variables to optimize the handle location.

4.3. Experiments

We performed two experiments to test the validity of the proposed objective function. This objective function is a simple model that neglects many of the biomechanical complexities of pushing during locomotion. The experiments described in this section are designed simply to test if the objective function captures broad features of natural human interaction with a rail, and to suggest how the objective function could be modified to better capture the notion of ease of manipulation. More experimental work is needed to further refine the model.

Static and dynamic experiments were performed. The experiments measured (1) the static force capabilities of subjects as they pushed on a stationary handle, to investigate the claim that subjects can apply larger pushing and pulling forces than sideways forces, and (2) the force profile as subjects pushed the load along a linear guide, to compare actual and predicted force profiles.

4.3.1. Static Force Capabilities

In this experiment we tested maximum static pushing and pulling force capabilities. This partially addresses the question of what humans can do during pushing and pulling of a cart, but it does not address what humans choose to do.

Subjects. Ten subjects, five male and five female, participated in the experiments. All subjects were graduate students with no knowledge of the purpose of the experiment. For each subject, the following data were collected: age, height, mass, elbow height, and knuckle height. All subjects were right-handed and between the ages of 22 and 38. Complete data for the subjects are given in the appendix.

Apparatus. The handle is a horizontally-mounted circular cross-section aluminum bar with a diameter of 1 in (2.54 cm). The center of the handle is 101 cm above the floor. The handle is fixed to a JR3 force sensor, which is mounted on a steel bracing on a wall-mounted full height cabinet. Subjects' hands on the handle are separated by approximately 7.5 cm.

Forces applied by the subject are displayed on a computer monitor on a shelf in the cabinet. The monitor is approximately eye-level so the subject can easily see the forces being applied. Forces in the horizontal plane only are displayed. The current force is displayed as a vector from the origin, with the up direction on the screen corresponding to forward forces (in the $+y$ direction), and the right direction on the screen corresponding to forces to the right ($+x$). In addition to the current force, the screen also maintains the envelope of the maximum forces the user has applied in every direction. The envelope is represented by 120 points approximately equally spaced angularly.

Experimental Protocol. Subjects were asked to push on the handle with strong, steady forces, not quick impulsive forces.

Maximum static pushing and pulling forces are strongly dependent on the height of the handle, configuration of the feet, and posture of the subject; see, for instance, Al-Eisawi et al. (1999). In our experiment, subjects put the tips of their shoes on a line 14 cm behind the center of the handle. The

distance between the feet was chosen by the subject to be a comfortable standing or walking distance. To ensure high friction at the feet, subjects wore rubber-soled shoes and stood on a neoprene mat.

Subjects were asked not to move their feet or hands, nor to bend significantly at the waist, during the experiments. Other than this, subjects were allowed to apply forces however they desired to increase the maximum force envelope. In particular, subjects were allowed to lean.

After experimenting with the handle to learn how forces are displayed on the screen, subjects were asked to draw their maximum force envelope by quadrants, in the sequence 1, 2, 4, 3. To draw a quadrant envelope, subjects began by applying a maximum pushing or pulling force, then increased force to the right or left until the force was completely to the side. After a brief rest, they then reversed the process. After all four quadrants were completed, they had the opportunity to go over the entire curve one more time.

Results. The maximum force envelopes for the ten subjects are shown in Figure 11. In general, larger forces are available in the y direction than the x direction. It varies from subject to subject, but forces to the right and left are approximately equal, and forces forward and backward are approximately equal.

For each subject we performed a least-squares fit of the envelope data to the ellipse $w_1 f_x^2 + w_2 f_y^2 = c$, where c was chosen arbitrarily. This yielded a weight ratio w_1/w_2 for each subject. The minimum and maximum weight ratios were 1.12 to 5.82, belonging to subjects 2m and 3f, respectively. The other eight subjects fell in the range [1.48, 2.84] with a mean of 1.971 and a standard deviation of 0.416.

The results confirm that under the test conditions, larger forces can be applied in the y direction than the x direction. We note that forces in the y direction may be made more asymmetric about the x-axis by placing the feet closer to or further from the handle, and forces in the x direction may be increased by increasing the width between the feet. Also, during walking, the forces which the subject can apply depend on which foot is on the ground, or the relationship of the feet on the ground.

The next set of experiments was chosen to look at the changing forces applied to a load during motion.

4.3.2. Linear Guided Motion

In this experiment, the subjects pushed and pulled a load constrained to a linear guide. Forces applied by the user during the motion were collected to compare to results predicted by the objective function. The results show that the subjects took advantage of the constraint by applying forces normal to it.

Subjects. Five subjects participated in the experiments. All participants were university students with no knowledge of the purpose of the experiments.

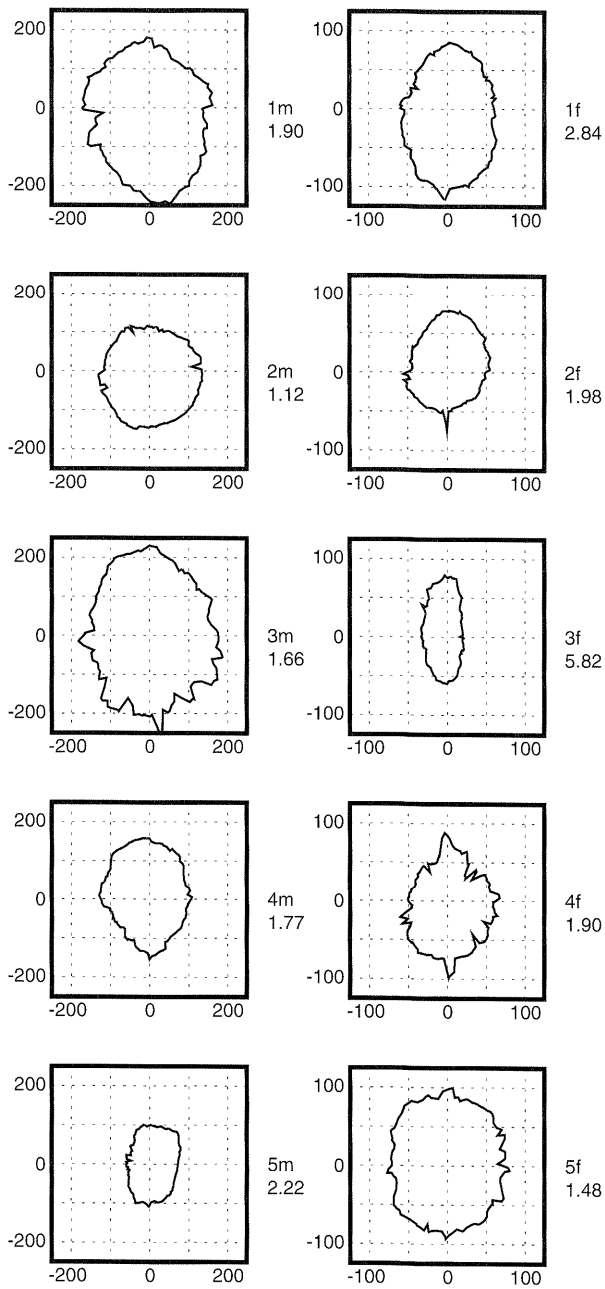

Fig. 11. Maximum force envelopes for ten subjects. The five subjects on the left are males (1m–5m), and the five subjects on the right are females (1f–5f). Units are Newtons. The max range for all male subjects is 250N, and the max range for all female subjects is 125N. Along with each plot is the weight ratio obtained by fitting an ellipse to the plot.

Apparatus. We have performed experiments in guided linear pushing using the Scooter tricycle cobot (Wannasuphoprasit et al. 1997), and using a trolley moving on a fixed overhead rail system (Figure 12). The fixed rail system is convenient for providing a very rigid constraint for testing purposes. The results we report in this paper are for the rail system.

The trolley handle is a circular cross-section aluminum bar with a diameter of 1 in (2.54 cm), and the center of the handle is 101 cm above the floor. The operator's hands on the handle are separated by approximately 7.5 cm. Forces at the handle are collected by a PC at 1000 Hz. The force sensor is an ATI Industrial Automation Gamma 15/50 force sensor. The sensor can measure forces in the y direction (forward in the human frame) in a range from -50 lb to 50 lb (-223 N to 223 N), and in the x (right) and z (up) directions in the range -15 lb to 15 lb (-67 N to 67 N). The mass of the moving trolley is approximately 75 kg. At slow walking speeds, the friction force on the trolley is approximately 7 N.

Experimental Protocol. We experimented with linear guides at angles $\alpha \in \{45°, 60°, 75°, 90°, 105°, 120°, 135°\}$ in the handle frame (Figure 13). Different angles are obtained by leaving the guide fixed and rotating the handle. Experiments were performed at two different motion distances, 72 in (183 cm) and 108 in (274 cm). The subjects performed each push and pull in three different manners:

- Pushing and pulling as comfortably as possible.
- Pushing and pulling comfortably while keeping the shoulders square to the handle.
- Pushing and pulling comfortably while keeping the elbows fully extended (locked), ensuring that the shoulders are square to the handle.

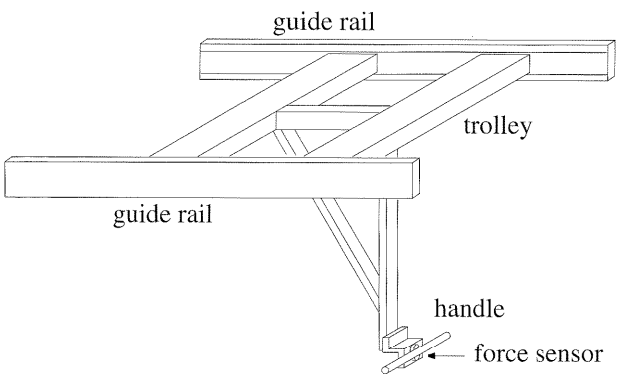

Fig. 12. A trolley on an overhead rail system provides a smooth rigid constraint.

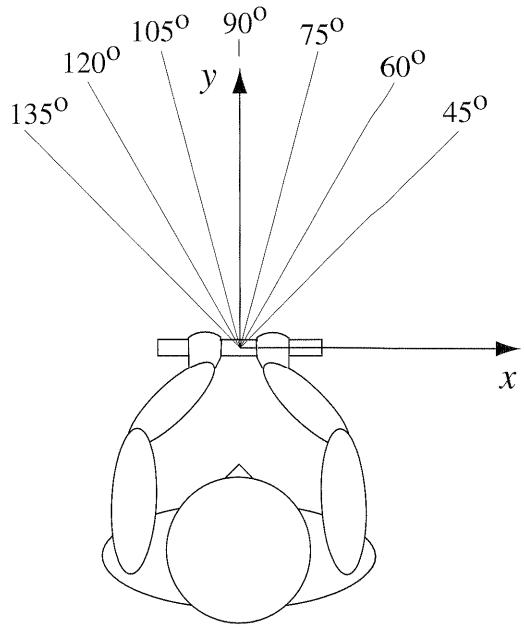

Fig. 13. Linear motion guides in the handle frame.

The last two manners were included to satisfy the assumption that the shoulders stay square relative to the handle. In the first manner, subjects tend to line up the shoulders perpendicular to the direction of locomotion.

For each combination of guide angle, pushing distance, and pushing manner, the subject was instructed to first practice a couple of times to feel comfortable with the guide. Then the subject was instructed to push the load forward to the final position in 2–3 seconds, rest for 2–3 seconds, and pull the load back to the initial position in 2–3 seconds.

Results. We report the results for a female volunteer, aged 20. The physiological data are:

Mass	68 kg
Height	170 cm
Shoulder height	135 cm
Elbow height	114 cm
Knuckle height	84 cm

Force data collected from four different trials are shown in Figure 14. The force profiles obtained with this subject are representative of results obtained with the other four subjects.

Forces in the y direction take an approximately ramp-like profile, as predicted by the objective function (eq. (6)) when interacting with a linear constraint. Although the forces quickly increase from zero to near their maximum value, this takes nonzero time. In our simple quadratic objective function of the applied force, there is no cost for a discontinuous

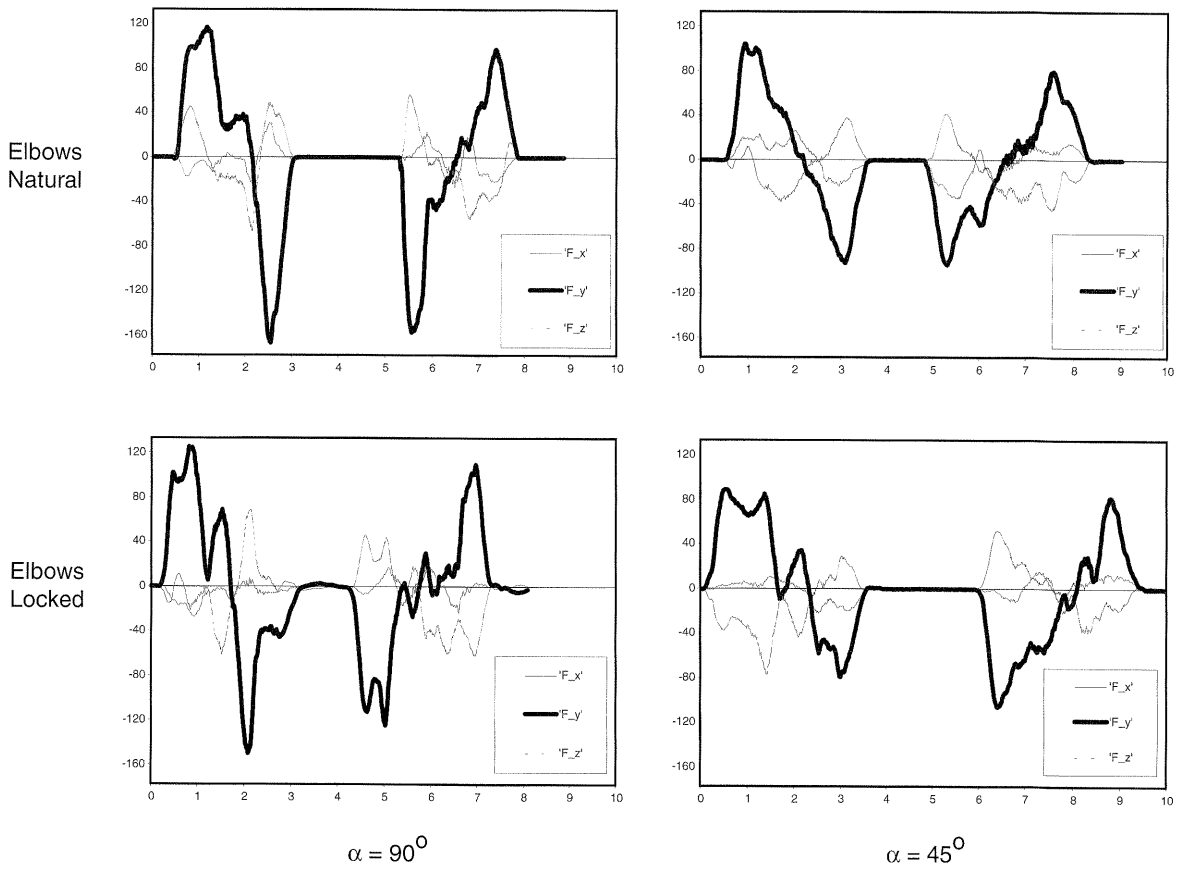

Fig. 14. Force (N) vs. time (s) from four representative pushing and pulling trials for a single subject. The results in the top row are for shoulders square and elbows in a natural position during pushing, and the results in the bottom row are for elbows locked straight. Results in the left column are for straight-ahead pushes ($\alpha = 90°$) and results in the right column are for a guide at $\alpha = 45°$ in the human frame.

change in force, and as a result the predicted forces have discontinuities at the beginning and end of the motion. A rate of change of force term could be added to the objective function.

We did not observe a significant increase in forces applied in the x direction as the angle α moved away from 90°. According to our simple model, this implies a large weight ratio w_1/w_2. In other words, the subjects made use of the constraint by applying forces normal to the constraint. This preliminary data supports the idea that a constraint can make a materials-handling task more comfortable for a human.

The motions are short enough that the subject does not achieve full-speed walking. With longer motions, we expect the subject will maintain a constant speed during the middle of the motion, providing just enough force to overcome friction at this speed. We could augment our simple model to include a walking velocity term. Note also that the integral of the pushing and pulling forces during a single motion are not equal. This is due to friction.

Maximum pulling forces tend to be larger than maximum pushing forces. When the subject pushes, there are significant downward forces, and when the subject pulls, there are significant upward forces (not considered in the planar model). This may be due to the fact that the hands are below the shoulders, and forces tend to act along the line defined by the hands and the shoulders. The force profiles with locked elbows are less smooth than those where the elbows are allowed to bend naturally. We suppose this is because bending the elbows absorbs variations in the force. When the elbows are locked, force variations are directly transmitted from the cyclical stepping motions.

Finally, we should note that the objective function (eq. (6)) is essentially a static model. It assumes that the subject's shoulders are fixed relative to the handle, and the subject walks at an angle determined by α. This may be a bit awkward, and in practice, if the angle is constant and the walking distance is sufficiently long, subjects tend to align the shoulders

perpendicular to the direction of motion. This simple model is just our first step at understanding the complex coordinated problem of pushing and locomoting.

5. Example: Guided Arm Motion

The framework of Section 3 can be applied to the problem of guiding multijoint human arm motions. This problem is attractive because it is far less biomechanically complex, and unconstrained reaching motions have been heavily studied in the human motor control literature, yielding several proposed "efficiency of motion" objective functions (Flash and Hogan 1985, Hollerbach and Atkeson 1987, Uno et al. 1989, Ma and Zahalak 1991, Alexander 1997, Harris and Wolpert 1998, Todorov and Jordan 1998). To test the benefit of using a motion guide in this new domain, we will adopt the minimum torque-change model proposed by Uno et al. (1989).[2]

The minimum torque-change model hypothesizes that natural human motions minimize the rate of change of torque

$$c = \frac{1}{2}\int_0^{t_f} \sum_{i=1}^{n} \left(\frac{d\tau_i}{dt}\right)^2 dt,$$

where τ_i is the torque at the ith joint. As in Uno et al. (1989), we will consider a two-joint ($i = 2$) robotic manipulator representing the shoulder-arm-hand system moving in a horizontal plane (Figure 15). Following Uno et al. (1989), the equations of motion are

$$\begin{aligned}
\tau_1 &= (I_1 + I_2 + 2m_2 l_1 s_2 \cos\theta_2 + m_2 l_1^2)\ddot{\theta}_1 \\
&\quad +(I_2 + m_2 l_1 s_2 \cos\theta_2)\ddot{\theta}_2 \\
&\quad -m_2 l_1 s_2 (2\dot{\theta}_1 + \dot{\theta}_2)\dot{\theta}_2 \sin\theta_2 + b_1\dot{\theta}_1 \\
\tau_2 &= (I_2 + m_2 l_1 s_2 \cos\theta_2)\ddot{\theta}_1 + I_2\ddot{\theta}_2 \\
&\quad +m_2 l_1 s_2 \dot{\theta}_1^2 \sin\theta_2 + b_2\dot{\theta}_2,
\end{aligned}$$

where m_i, I_i, l_i, s_i are the mass, inertia about the joint, length, and distance from the joint to the center of mass of link i. b_i is the viscous friction coefficient at joint i. The values of these physical parameters are taken from Uno et al. (1989) and reproduced in Table 1.

If the hand is holding a load m_l, we can consider it a part of link 2. The mass of link 2 becomes $m_2' = m_2 + m_l$, the inertia becomes $I_2' = I_2 + m_l l_2^2$, and the distance to the center of mass becomes $s_2' = (m_2 s_2 + m_l l_2)/(m_2 + m_l)$.

We study a reaching motion with a load $m_l = 1$ kg from (0.2 m, 0.3 m) to (0, 0.5 m) in a frame centered at the shoulder. The time of motion is 1 s. We begin by using our numerical method to recover essentially the same results as Uno et al. (1989) for the case of unconstrained motion. Then, to demonstrate the benefit of a guide, we show that the same trajectory can be executed at a significantly lower cost if a guide constrains the motion to the path. Finally, we replace the near-linear path found in the unconstrained case by a linear guide and derive the optimal human interaction with the guide.

In this problem, a guide at the load in the hand is equivalent to a guide in joint space, as the inverse kinematics from hand positions to arm joint configurations is smooth and one-to-one.

2. The use of this model is not meant as an endorsement over other models. It is simply used to test the problem formulation with a different type of objective function.

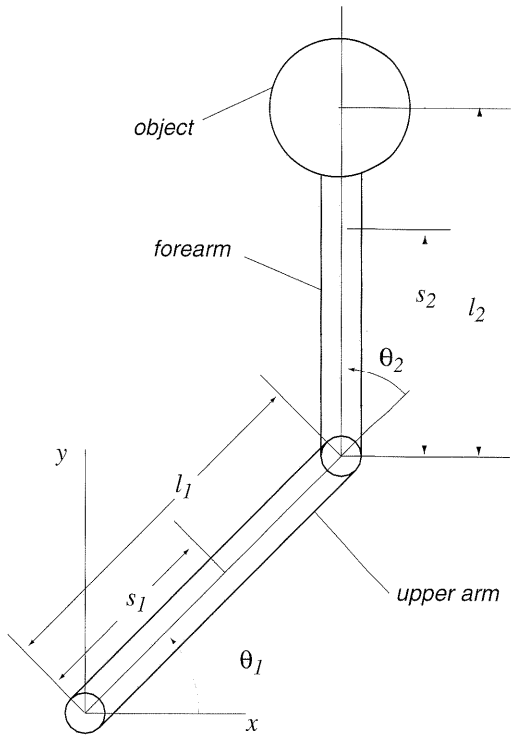

Fig. 15. The two-joint robotic model of the human shoulder and elbow.

Table 1. Physical Parameters for the Two-Joint Manipulator

Parameter	Link 1	Link 2
m_i (kg)	0.9	1.1
I_i (kg m^2)	0.065	0.100
l_i (m)	0.25	0.35
s_i (m)	0.11	0.15
b_i (kg m^2/s)	0.08	0.08

5.1. Unconstrained Motion

The design variables to the optimization are the coefficients of sixth-order polynomials of time describing $\theta_1(t)$ and $\theta_2(t)$.

Constraints on these coefficients place the end-effector of the manipulator at the start and goal locations at $t = 0$ and $t = 1$s, respectively, at zero velocity.

The results of the optimization are shown in Figures 16 and 17. The motion is nearly a straight line with a bell-shaped velocity curve, as predicted by Uno et al. (1989). Natural reaching motions have been experimentally observed to have these properties (Morasso 1981, Abend et al. 1982, Flash and Hogan 1985, Hollerbach and Atkeson 1987, Uno et al. 1989). The cost of the simulated motion is 60 (units suppressed).

We denote the optimized trajectory as $\Theta_u(t)$ with joint torques $\tau_u(t)$, where "u" indicates unconstrained.

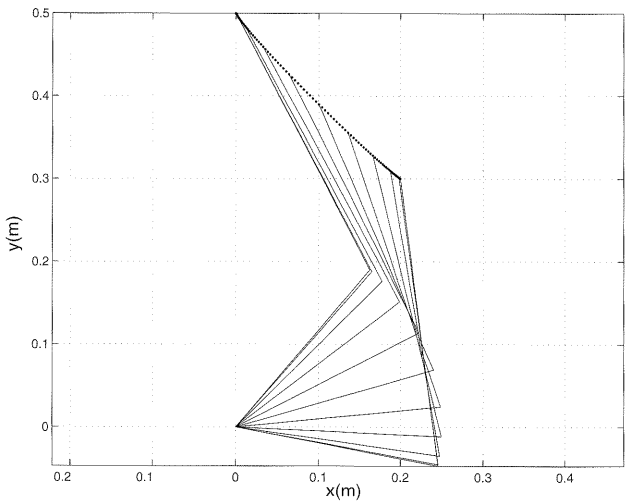

Fig. 16. The optimal unconstrained arm motion.

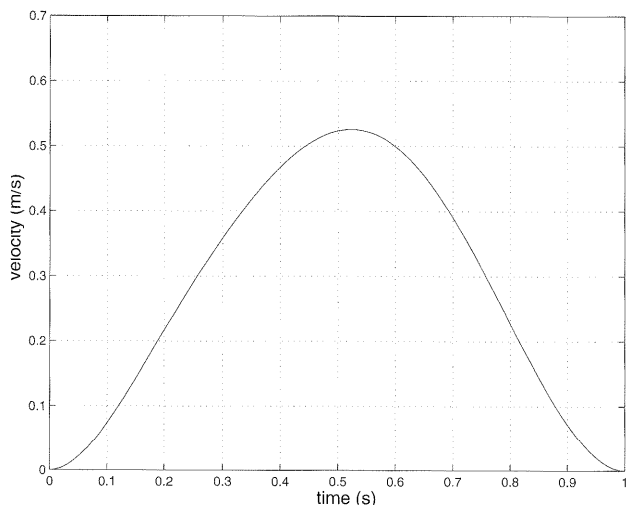

Fig. 17. The speed of the hand vs. time during the optimal motion is bell-shaped.

5.2. Constrained Motion

The presence of a guide along the path of Figure 16 allows the human to apply forces against the guide in order to reduce the objective function. Forces normal to the guide do not affect the trajectory.

At an arm velocity $(\dot{\theta}_1, \dot{\theta}_2)^T$, arm torques normal to the guide have the form $\alpha(-\dot{\theta}_2, \dot{\theta}_1)^T$. We define $\tau_n(t)$ to be the torques normal to the guide the human adds to $\tau_u(t)$ to minimize the cost. Let $\tau_n(t)$ be a sixth-order polynomial function of time

$$\tau_n(t) = \begin{pmatrix} -\dot{\theta}_2(t) \\ \dot{\theta}_1(t) \end{pmatrix} \sum_{i=0}^{6} c_i t^i, \quad 0 \le t \le t_f = 1.$$

Keeping the trajectory $\Theta_u(t)$, the cost of the manipulation is the integral of the change of torque squared of $\tau_u(t) + \tau_n(t)$. We solve for the optimal set of c_i and find the cost is reduced to 31. In this case, even with the same trajectory, the cost of the manipulation can be halved by the use of a guide.

Our next step was to keep the guide associated with $\Theta_u(t)$, but to allow the operator to move along the guide at any speed. We solved for the optimal sixth-order polynomial time-scaling $s(t)$ along the path in addition to the optimal torque profile $\tau_n(t)$, and we found that by altering the speed along the path slightly from that in $\Theta_u(t)$, the cost could be further lowered to 26.

The torque profiles for the optimal motions in the unconstrained case, same trajectory with a guide, and same path with a guide, are given in Figure 18. It is apparent that the rate of change of τ_1 and τ_2 is less with the guide than without, explaining the decrease in the objective function.

Finally, we replaced the path of $\Theta_u(t)$ by the linear guide

$$\begin{aligned} x(s) &= x_0 - \frac{1}{\sqrt{1+k^2}} s \\ y(s) &= y_0 - \frac{k}{\sqrt{1+k^2}} s, \end{aligned}$$

where $s \in [0, \sqrt{(x_f - x_0)^2 + (y_f - y_0)^2}]$ is an arclength parameterization of the guide, $k = (y_f - y_0)/(x_f - x_0)$ is the slope, and $(x_0, y_0) = (0.2\text{m}, 0.3\text{m})$ and $(x_f, y_f) = (0, 0.5\text{m})$. Any time-scaling $s(t)$ implies a trajectory $\Theta_p(t)$ and an associated set of joint torques $\tau_p(t)$. We solve for the sixth-order polynomials $s(t)$ (subject to initial and terminal constraints) and the added normal torques $\tau_n(t)$ to minimize the cost of the joint torques $\tau_p(t) + \tau_n(t)$. The result is similar to the previous result, with a cost of 25, since the path associated with $\Theta_u(t)$ is nearly linear. The forces applied by the human normal to the guide during the motion are shown in Figure 19.

In future work, we plan to conduct human experiments with a linear guide to see how accurately various objective functions predict the interaction. Most existing hypotheses target the unconstrained case, so a new hypothesis may have to be formulated for the constrained case.

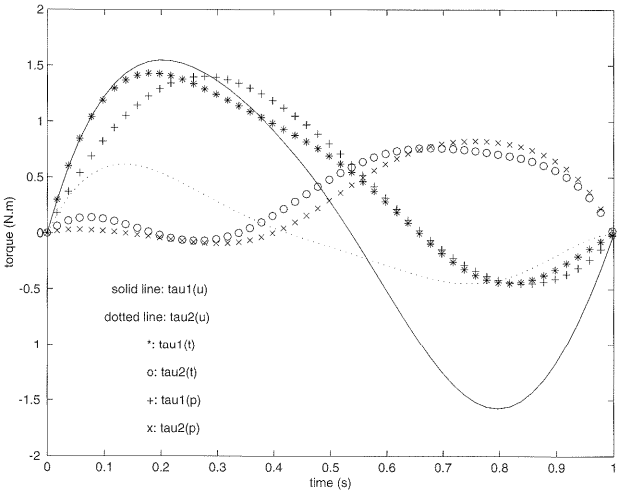

Fig. 18. Joint torques for the optimal unconstrained motion (u), motion along the same trajectory with a guide (t), and motion along the same path with a guide (p).

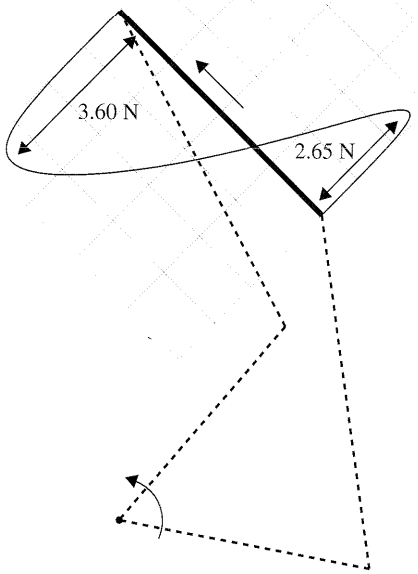

Fig. 19. Forces applied normal to the linear guide during optimal constrained arm motion.

6. Discussion and Future Work

This paper has formulated the problem of designing passive motion guides for assisted manipulation and has applied the formulation to two different task domains. Our current and future experimental work is aimed at gaining a better understanding of natural human interaction with guiding constraints. This understanding is crucial to designing comfortable motion guides. This experimental work will inform us if models of unconstrained human motion may be adapted to the constrained case, or if new theories of constrained motion must be developed.

Although our current work is studying natural constrained motions of subjects, it is clear that the natural motion strategies adopted by humans are not always the safest. For example, humans often lift heavy boxes by bending at the lower back, and it requires conscious effort or training to lift with the legs to protect the back. Motion guides can be designed so that the natural interaction with them leads to a safe motion strategy. They can also be used to vary the motion to prevent cumulative trauma disorders, or as training devices.

Because guiding constraints are purely passive, they are incapable of injecting energy into the load, as is required when lifting a load in a gravity field. This paper has focused on pushing and pulling tasks, and other approaches to assisted manipulation may be more appropriate for lifting tasks. However, weightlifters can lift heavier weights if they are confined to a rail, and a programmable rail could allow the user to use smaller forces to build up energy in the load by pushing horizontally (or even downward) before the motion is directed upward.

At certain postures of the body, it may be difficult for the operator to apply wrenches to the load in certain directions. If the space of feasible operator wrenches is orthogonal to the current motion of the load, the operator is incapable of speeding up or slowing down the motion. The operator "loses control" of the motion. If it is necessary to rule out this possibility, we can place constraints on the shape of the guide. To allow motion to be stopped in case of emergency, the system could also be equipped with brakes. The addition of brakes does not affect the passivity of the device, but it relieves the human of effort to decelerate the load.

Although this paper has focused on guides with a single degree-of-freedom, it is easy to imagine guides that constrain the load to a multi-dimensional manifold (smaller than the full configuration space of the load). A guide may eliminate some degrees-of-freedom that are problematic for the operator, while leaving others free for the operator to use as desired. Unilateral constraints on the configuration space can also be used to "funnel" the motion of the load. We hypothesize that in most circumstances, manipulation becomes easier for the operator as more constraints are added, provided the constraints are tailored to the operator.

Table A1. Subject Data for Static Force Experiments

Subject	Sex	Age	Height (cm)	Mass (kg)	Elbow (cm)	Knuckle (cm)
1m	M	29	173	102	107	74
2m	M	27	182	66	112	76
3m	M	26	184	92	112	79
4m	M	30	168	70	105	76
5m	M	32	170	74	100	66
1f	F	38	159	50	102	71
2f	F	33	160	48	98	69
3f	F	23	161	54	100	69
4f	F	26	147	41	93	64
5f	F	24	158	50	102	72

Another interesting possibility is to adapt the motion guide based on the operator interaction with it. This would allow the motion guide to be customized to each user. Instead of simply modifying a single guide, it may also be possible to modify the objective function based on the interaction, allowing the design of other guides for the particular user. This is a subject of ongoing research.

Finally, designing motion guides is a path planning problem with dynamics and a cost function based on human effort. The nonlinear programming approach described in this paper will likely encounter convergence problems in cluttered spaces if obstacles are included as nonlinear inequality constraints. Guides through tight spaces could be assembled from a small set of near-optimal guide primitives, either manually or by automatic motion planning.

Appendix: Subject Data

Table A1 gives the physiological data for the ten subjects in the static force experiments of Section 4.3.1.

Acknowledgments

We thank Tetsuo Kotoku, Etienne Burdet, Andy Ruina, Art Kuo, Mitsuo Kawato, Hiroaki Gomi, Jules Dewald, and Sandro Mussa-Ivaldi for discussions on the ideas in this paper, and the anonymous reviewers for their suggestions. This work was funded by NSF grants IIS-9875469 and IIS-0082957.

References

Abend, W., Bizzi, E., and Morasso, P. 1982. Human arm trajectory formation. *Brain* 105:331–348.

Adams, M. A., and Hutton, W. C. 1983. The effect of fatigue on the lumbar intervertebral disc. *Journal of Bone and Joint Surgery* 65-B:199–203.

Al-Eisawi, K. W., Kerk, C. J., Congleton, J. J., Amendola, A. A., Jenkins, O. C., and Gaines, W. G. 1999. The effect of handle height and cart load on the initial hand forces in cart pushing and pulling. *Ergonomics* 42(8):1099–1113.

Al-Jarrah, O. M., and Zheng, Y. F. 1996. Arm-manipulator coordination for load sharing using compiant control. In *IEEE International Conference on Robotics and Automation* pp. 1000–1005.

Alexander, R. M. 1997. A minimum energy cost hypothesis for human arm trajectories. *Biological Cybernetics* 76:97–105.

Arai, H., Takubo, T., Hayashibara, Y., and Tanie, K. 2000. Human-robot cooperative manipulation using a virtual nonholonomic constraint. In *IEEE International Conference on Robotics and Automation*.

Ayoub, M. M., and Dempsey, P. G. 1999. The psychophysical approach to manual materials handling task design. *Ergonomics* 42(1):17–31.

Brinkman, P. 1986. Injury of the annulus fibrosis and disc protrusions. *Spine* 11:149–153.

Bryson, A. E., and Ho, Y.-C. 1969. *Applied Optimal Control.* Blaisdell.

Ciriello, V. M., McGorry, R. W., Martin, S. E., and Bezverkhny, I. B. 1999. Maximum acceptable forces of dynamic pushing: Comparison of two techniques. *Ergonomics* 42(1):32–39.

Flash, T., and Hogan, N. 1985. The coordination of arm movements: an experimentally confirmed mathematical model. *Journal of Neuroscience* 5(7):1688–1703.

Gill, P. E., Murray, W., and Wright, M. H. 1981. *Practical Optimization.* New York: Academic Press.

Gomi, H., and Kawato, M. 1995. Task dependent stiffness of human multi-joint arm during point-to-point movement. Isrl-95-4, NTT Basic Research Laboratories.

Gomi, H., and Kawato, M. 1996. Equilibrium-point control hypothesis examined by measured arm stiffness during multijoint movement. *Science* 272:117–120.

Gomi, H., and Kawato, M. 1997. Human arm stiffness and equilibrium-point trajectory during multi-joint movement. *Biological Cybernetics* 76:163–171.

Granata, K. P., and Marras, W. S. 1999. Relation between spinal load factors and the high-risk probability of occupaional low-back disorder. *Ergonomics* 42(9):1187–1199.

Harris, C. M., and Wolpert, D. M. 1998. Signal-dependent noise determines motor planning. *Nature* 394(20):780–784.

Hayashibara, Y., Tanie, K., Arai, H., and Tokashiki, H. 1997. Development of power assist system with individual compensation ratios for gravity and dynamic load. In *IEEE/RSJ International Conference on Intelligent Robots and Systems*, pp. 640–646.

Hogan, N. 1984. Adaptive control of mechanical impedance by coactivation of antagonist muscles. *IEEE Transactions on Automatic Control* 29(8):681–690.

Hogan, N. 1985. The mechanics of multi-joint posture and movement control. *Biological Cybernetics* 52:315–331.

Hollerbach, J. M., and Atkeson, C. G. 1987. Deducing planning variables from experimental arm trajectories: Pitfalls and possibilities. *Biological Cybernetics* 56:279–292.

Homma, K., and Arai, T. 1995. Design of an upper limb motion assist system with parallel mechanism. In *IEEE International Conference on Robotics and Automation*, pp. 1302–1307.

Kazerooni, H. 1990. Human-robot interaction via the transfer of power and information signals. *IEEE Transactions on Systems, Man, and Cybernetics* 20(2):450–463.

Kazerooni, H. 1996. The human power amplifier technology at the University of California, Berkeley. *Journal of Robotics and Autonomous Systems* 19:179–187.

Kim, K. I., and Zheng, Y. F.1998. Human-robot coordination with rotational motion. In *IEEE International Conference on Robotics and Automation*, pp. 3480–3485.

Kirk, D. E. 1970. *Optimal Control Theory*. Prentice-Hall Inc.

Kosuge, K., Fujisawa, Y., and Fukuda, T. 1993. Mechanical system control with man-machine-environment interactions. In *IEEE International Conference on Robotics and Automation*, pp. 239–244.

Kram, R. 1998. Metabolic energy consumption during animal locomotion. In *Allerton Conference on Communication, Control, and Computing*, pp. 757–764.

Krylow, A. M., and Rymer, W. Z. 1997. Role of intrinsic muscle properties in producing smooth movements. *IEEE Transactions on Biomedical Engineering* 44(2):165–176.

Lawrence, C., Zhou, J. L., and Tits, A. L. 1994. *User's Guide for CFSQP Version 2.3.* Institute for Systems Research 94-16, University of Maryland.

Legg, S. J., and Myles, S. W. 1981. Maximum acceptable repetitive lifting workloads for an 8 hour work-day using psychophysical and subjective rating methods. *Ergonomics* 24:907–916.

Ma, S., and Zahalak, G. I. 1991. A distribution-moment model of energetics in skeletal muscle. *Journal of Biomechanics* 24:21–35.

Marras, W. S., Granata, K. P., Davis, K. G., Allread, W. G., and Jorgensen, M. J. 1999. Effects of box features on spine loading during warehouse order selecting. *Ergonomics* 42(7):980–996.

Mital, A. 1983. The psychophysical approach in manual lifting—A verification study. *Human Factors* 25:485–491.

Morasso, P. 1981. Spatial control of arm movements. *Experimental Brain Research* 42:223–227.

Nagai, K., Nakanishi, I., Hanafusa, H., Kawamura, S., Makikawa, M., and Tejima, N. 1998. Development of an 8DoF robotic orthosis for assisting human upper limb motion. In *IEEE International Conference on Robotics and Automation*, pp. 3486–3491.

National Institute for Occupational Safety and Health. 1981. *Work Practices Guide for Manual Lifting*, NIOSH publication no. 81-122.

Nelson, W. L. 1983. Physical principles for economies of skilled movements. *Biological Cybernetics* 46(2):135–47.

Peshkin, M., Colgate, J. E., Wannasuphoprasit, W., Moore, C., and Gillespie, B. 2000. Cobot architecture. *IEEE Transactions on Robotics and Automation.*

Shirazi-Adl, A., Ahmed, A. M., and Shrivastava, S. C. 1986. Mechanical response of the lumbar motion segment in axial torque alone and in combination with compression. *Spine* 11:914–927.

Snook, S. H., and Ciriello, V. M. 1991. The design of manual handling tasks: revised tables of maximum acceptable weights and forces. *Ergonomics* 34:1197–1213.

Takubo, T., Arai, H., and Tanie, K. 2000. Virtual nonholonomic constraint for human-robot cooperation in 3-D space. In *IEEE/RSJ International Conference on Intelligent Robots and Systems*, Takamatsu, Japan.

Todorov, E., and Jordan, M. I. 1998. Smoothness maximization along a predefined path accurately predicts the speed profiles of complex arm movements. *Journal of Neurophysiology* 80(2):696–714.

Uno, Y., Kawato, M., and Suzuki, R. 1989. Formation and control of optimal trajectory in human multijoint arm movement. *Biological Cybernetics* 61:89–101.

Wannasuphoprasit, W., Gillespie, R. B., Colgate, J. E., and Peshkin, M. A. 1997. Cobot control. In *IEEE International Conference on Robotics and Automation*, pp. 3571–3577.

Yamamoto, Y., Eda, H., and Yun, X. 1996. Coordinated task execution of a human and a mobile manipulator. In *IEEE International Conference on Robotics and Automation.*